IEEE Access
Multidisciplinary ⋮ Rapid Review ⋮ Open Access Journal

Received June 30, 2020, accepted July 24, 2020, date of publication July 30, 2020, date of current version August 14, 2020.

Digital Object Identifier 10.1109/ACCESS.2020.3013000

Simulation of HVDC System Steady and Transient Response by an Analytical Method

CHONGTAO LI[1], YONG ZHAO[2], FENG ZENG[1], AND ZHENGCHUN DU[1], (Member, IEEE)
[1]Department of Electrical Engineering, Xi'an Jiaotong University, Xi'an 710049, China
[2]Electric Power Research Institute, CSG, Guangzhou 510080, China

Corresponding author: Chongtao Li (lichongtao@mail.xjtu.edu.cn)

This work was supported in part by the National Key Research and Development Program Projects under Grant 2017YFB0902000, and in part by the National Natural Science Foundation of China under Grant 51507127.

ABSTRACT This paper proposes an analytical method for simulation of the steady and transient response of the HVDC system in order to simulate the electromagnetic process of HVDC system in the simulation of hybrid AC/DC system. First, the boundaries of AC and DC systems as well as some assumptions are introduced. Then, the HVDC system is considered as a combination of primary equipment sub-systems (PES) and control sub-systems (CS). According to the assumptions, the PES can be represented by different homogeneous linear differential equations within different time intervals that are determined by the status of converters. These equations can be solved in analytical method. The CS is expressed by nonlinear differential and algebraic equations and simulated in numerical integration method. The interface parameters of each module are also introduced. The accuracy and efficiency of the proposed model are verified by comparing the simulation results computed by the proposed model with that simulated in PSCAD.

INDEX TERMS AC/DC hybrid system simulation, HVDC, electromagnetic transient process, commutation failure.

I. INTRODUCTION

Employing the high-voltage direct-current (HVDC) systems for transmitting power over long distances has become a trend. The introduction of HVDC transmission systems in an alternating-current (AC) system has led to the concept of hybrid AC/DC systems. With line-commutated thyristor converters widely adopted, commutation failures may occur due to the symmetric and asymmetric AC faults [1], [2]. Continuous commutation failures may cause a converter block, which leads to a potential power transfer from DC to AC lines. As a result, AC systems might develop some stability problems [3], [4].

Detailed models of AC and DC systems should be adopted to simulate the interaction of AC and DC systems' transients. The well-developed transient stability simulation techniques of AC systems adopt a quasi-steady state model [5] of the AC network where only fundamental components are used to reduce computational burden. This model best captures the electro-mechanical behavior of AC systems. Response models, where the dynamics of the pole controls are neglected, are often adopted for DC systems [6]. The commutation failure is approximately checked by monitoring the AC bus voltage, extinction angle, etc. [4], [7], which is computed by a quasi-steady state model.

In order to capture the detailed dynamic behavior of an HVDC system for the purpose of analyzing the stability of AC/DC hybrid systems, it is better to adopt the electromagnetic model [7], [8], which takes into account the explicit dynamics of the converters, DC lines, etc. For the electromagnetic simulation of HVDCs, the integration step needs to be selected in microseconds to capture an accurate response. However, large integral steps, like half of the AC voltage cycle, are generally adopted in the transient simulations of AC systems. This leads to different simulation time scales. A multirate simulation technique has been proposed for simulating systems containing a wide range of time scales [9]. In this technique, any suitable integration algorithm, with fixed or variable time-step, can be applied to the fast and/or slow sub-systems. Simulations of hybrid transient stability and electro-magnetic transient have also been studied [10], [11].

A general way to derive the dynamic behavior of HVDC systems in hybrid simulations, is simulating by available software packages, like EMTP, PSCAD/EMTDC,

The associate editor coordinating the review of this manuscript and approving it for publication was Yonghao Gui.

or MATLAB/SIMULINK. In these packages, validated models are available for power system studies. EMTP and PSCAD/EMTDC adopt the nodal analysis simulation tool, while MATLAB/SIMULINK utilizes the state-space model [12]. The simulation techniques in these tools are basically numerical integration methods, like trapezoidal integration [12], Backward Euler [13], multistep method [14], etc. Fixed integration step or variable time-step can also be used.

As we know, truncation error is an inherited problem of the numerical integration method. Moreover, interpolation and reinitialization techniques are normally adopted in simulating transients of power electronics with switching circuits to reduce numerical oscillations [15]. For specific studies, some other methods may obtain better results. For example, an analytical method is introduced in [16] to compute the steady-state response of HVDCs, which can theoretically obtain more accurate results since there is no truncation error. By computing the exact circuit switching time, numerical oscillation can be avoided in this method.

In this paper, an HVDC model for stability and electromagnetic transient simulations of AC/DC hybrid systems is proposed. The main purpose of this new model is to simulate the detailed transient behavior of HVDCs under AC system faults for stability analysis of AC/DC hybrid systems. In the proposed model, the HVDC system is represented by PES and CS. The dynamical behavior of the PES is fast. Thus, the analytical method is applied to compute the response of PES. Compared with numerical integration method, truncation error will not exist in analytical method, and numerical oscillation can be avoided since the exact circuit switching time can be computed. Moreover, in analytical method, the integration step is not a limitation. Since the dynamical behavior of CS is slow, the response is calculated by numerical integration method. The PES and CS have some variables exchanging in the simulation, which are introduced in section III. In conclusion, we search for a new simulation method to simulate the dynamical behavior of HVDC in a hybrid AC/DC system. Since the analytical method is applied, it is expected with more accurate results, no numerical oscillation and faster in computational time.

II. ASSUMPTIONS

The schematic diagram of a 12-pulse HVDC system is shown in Fig. 1. In this paper, the boundary of AC and HVDC systems in a hybrid AC/DC system is selected as the converter bus.

The AC system includes all generators, loads, AC transmission lines, etc., where the networks are described using quasi-state model. The HVDC system includes the converter transformers, converters, DC lines, DC filters and smoothing reactors, which are modelled by RLC circuit model. The HVDC control system is also included.

This paper aims to find an effective mathematical model and simulation method of HVDCs for hybrid

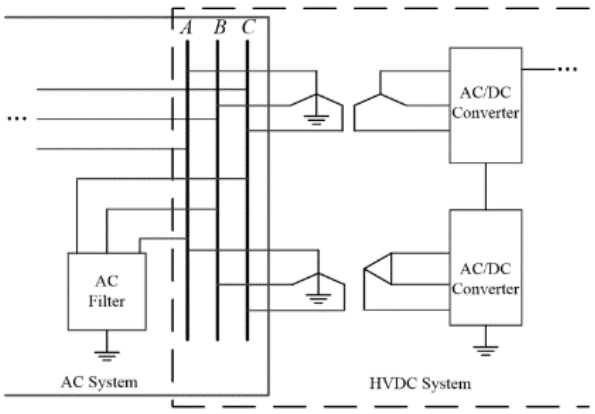

FIGURE 1. The boundary of AC and HVDC system.

electro-mechanical and electromagnetic transient simulations. Thus, the following assumptions are considered:

1.The effect of AC filters is ideal, i.e., the converter bus voltage is sinusoidal in an AC simulation step.

2.The excitation impedances of the converter transformers are ignored in the HVDC system and the saturation of the converter transformers is not considered.

For the second assumption, the excitation impedance of the converter transformer can be included in the AC system as a shunt impedance connected to the converter bus.

In real power systems, the total harmonic distortion of the bus voltage is limited to a low level, e.g., no more than 2%. As a result, harmonic components can be ignored. Moreover, the network function is described by quasi-steady state model in the AC system, which means that the voltages are represented as phasors (shown in Fig. 2). Thus, the assumptions are meaningful.

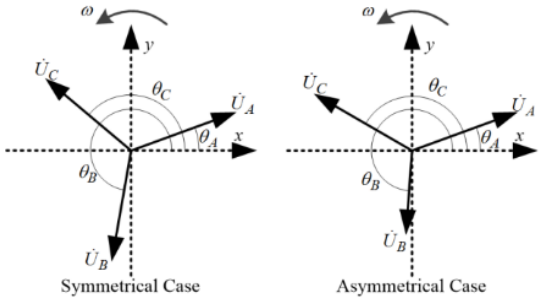

FIGURE 2. Bus voltages under symmetrical and asymmetrical cases. (x axis represents the reference axis of bus voltages).

Under the aforementioned assumptions, the bus voltages in time domain can be described as:

$$\begin{aligned} u_A &= U_A \cos(\omega t + \theta_A) \\ u_B &= U_B \cos(\omega t + \theta_B) \\ u_C &= U_C \cos(\omega t + \theta_C) \end{aligned} \tag{1}$$

where U_A, U_B and U_C are the amplitudes of the bus voltage; ω is the angular frequency of the bus; θ_A, θ_B and θ_C are the

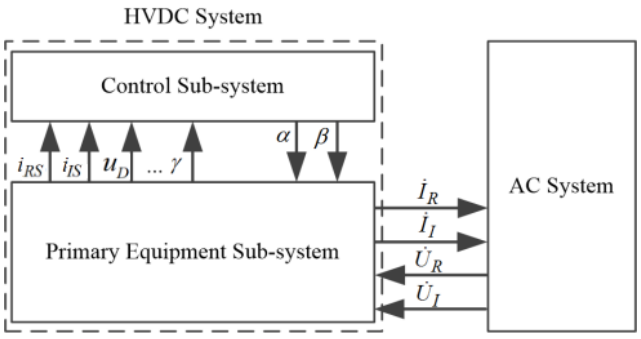

FIGURE 3. The structure of the HVDC system and the relationship between the mathematical models of the HVDC system and AC systems.

related phase angles. For symmetrical cases, the following assumptions are valid:

$$U_A = U_B = U_C \tag{2}$$

$$\theta_B - \theta_C = \theta_C - \theta_A = 2\pi/3 \tag{3}$$

III. STRUCTURE OF HVDC SYSTEM

The structure of the HVDC system is discussed in this section. The HVDC system is expressed by a PES and a CS, as shown in Fig. 3.

In the mathematical model, the AC system provides the converter bus voltages $\dot{U}_R$ and $\dot{U}_I$ to the PES through the AC system simulation, where the subscripts 'R' and 'I' denote the rectifier and inverter sides, respectively. PES returns the fundamental currents $\dot{I}_R$ and $\dot{I}_I$ to the AC system. Simultaneously, PES provides some variables to CS, such as the DC currents i_{RS} and i_{IS}, DC voltage u_D and extinction angle γ.

According to the control logic as well as the variables provided by PES, CS adjusts the delay angle α at the rectifier and advances angle β at the inverter, which will be sent to PES for triggering the thyristors.

IV. MODELLING AND SIMULATION OF THE PES

A schematic diagram of the PES is shown in Fig. 4. In both sides of the rectifier and inverter, there are components like converters, converter transformers, smoothing reactor and DC filter. The DC filter is a single-tuned filter. The DC line, which adopts the T-type equivalent circuit for simplicity, couples the rectifier to the inverter. A cascaded T-type equivalent circuit can also be adapted to obtain more accurate results. In the following part of this section, the state space representation of the PES is provided. Under the assumptions, the PES will be represented by linear homogeneous differential equations and solved by analytical method.

A. CONVERTERS, CONVERTER TRANSFORMERS AND SMOOTHING REACTOR

The converters, converter transformers and smoothing reactors in either the rectifier or inverter side will be considered as an entirety to formulate the model. The state function associated with this part is difficult to formulate, taking into account all 12 thyristor valves and their interconnections. It is then necessary to form the state function in terms of different commutation or conduction intervals. With the assumption of the ideal Y-Y and Y-Δ converter transformers, one of the equivalent circuits is shown in Fig. 5, where converter 1 is in the commutation interval and converter 2 is in the conduction interval.

The differential equations in Fig. 5 are represented as:

$$L_y \frac{d}{dt}\begin{bmatrix} i_{yA} \\ i_{yB} \\ i_{yC} \end{bmatrix} = k_y \begin{bmatrix} u_A \\ u_B \\ u_C \end{bmatrix} - \begin{bmatrix} v_{yA} \\ v_{yB} \\ v_{yC} \end{bmatrix} \tag{4}$$

$$L_d \frac{d}{dt}\begin{bmatrix} i_{dA} \\ i_{dB} \\ i_{dC} \end{bmatrix} = k_d \begin{bmatrix} u_A \\ u_B \\ u_C \end{bmatrix} - \begin{bmatrix} v_{dA} \\ v_{dB} \\ v_{dC} \end{bmatrix} \tag{5}$$

$$L_S \frac{di_S}{dt} = v_{yD} + v_{dD} - u_D \tag{6}$$

where k_y, k_d, L_y and L_d are the turns ratios and equivalent secondary inductances of the Y-Y and Y-Δ converter transformers, respectively.

The voltages and currents in (4)-(6) have the following relations:

$$\left.\begin{matrix} v_{yB} - v_{yC} = 0, & v_{yA} - v_{yB} - v_{yD} = 0 \\ v_{dA} - v_{dD} = 0, & v_{dA} + v_{dB} + v_{dC} = 0 \end{matrix}\right\} \tag{7}$$

$$\left.\begin{matrix} i_{dB} - i_{dC} = 0, & i_{yA} + i_{yB} + i_{yC} = 0 \\ i_S - i_{yA} = 0, & i_S + i_{dC} - i_{dA} = 0 \end{matrix}\right\} \tag{8}$$

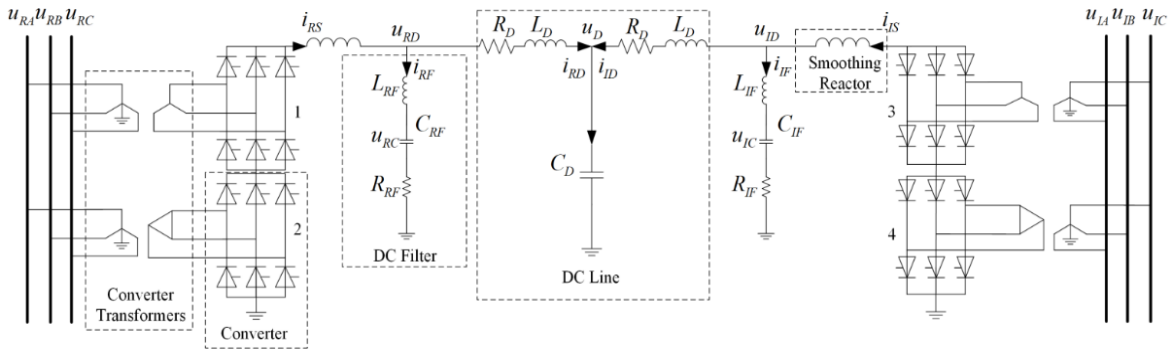

FIGURE 4. Schematic diagram of the PES.

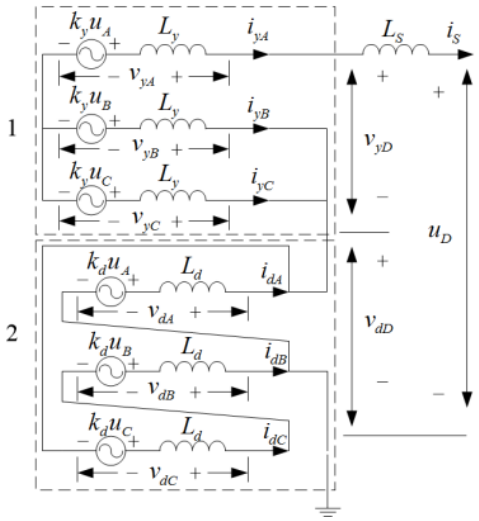

FIGURE 5. The equivalent circuit representation of the converters, converter transformers and smoothing reactor.

Differentiating equation (8) results in:

$$\begin{aligned} k_d u_B - v_{dB} - k_d u_C + v_{dC} &= 0 \\ k_y(u_A + u_B + u_C) - (v_{yA} + v_{yB} + v_{yC}) &= 0 \\ L_S(v_{yD} + v_{dD} - u_D) - L_y(k_y u_A - v_{yA}) &= 0 \\ L_d(v_{yD} + v_{dD} - u_D) - L_S(k_d u_A - v_{dA} - k_d u_C + v_{dC}) &= 0 \end{aligned} \tag{9}$$

Combining (4)-(7) and (9) results in:

$$\begin{bmatrix} \boldsymbol{T}_C d\boldsymbol{x}_C/dt \\ \boldsymbol{0} \end{bmatrix} = \begin{bmatrix} \boldsymbol{B}_{11} & \boldsymbol{B}_{12} \\ \boldsymbol{B}_{21} & \boldsymbol{B}_{22} \end{bmatrix} \begin{bmatrix} \boldsymbol{u} \\ \boldsymbol{v} \end{bmatrix} + \begin{bmatrix} \boldsymbol{b}_1 \\ \boldsymbol{b}_2 \end{bmatrix} u_D \tag{10}$$

where $\boldsymbol{x}_C = [i_{yA}\ i_{yB}\ i_{yC}\ i_{dA}\ i_{dB}\ i_{dC}\ i_S]^{\mathrm{T}}$; $\boldsymbol{u} = [u_A\ u_B\ u_C]^{\mathrm{T}}$; $\boldsymbol{v} = [v_{yA}\ v_{yB}\ v_{yC}\ v_{dA}\ v_{dB}\ v_{dC}\ v_{yD}\ v_{dD}]^{\mathrm{T}}$; $\boldsymbol{T}_C, \boldsymbol{B}_{11}, \boldsymbol{B}_{12}, \boldsymbol{B}_{21}, \boldsymbol{B}_{22}, \boldsymbol{b}_1$ and $\boldsymbol{b}_2$ are the corresponding coefficient matrices. For detailed contents in the matrices, please see Appendix A.

Eliminating $\boldsymbol{v}$ in (10) yields:

$$\frac{d\boldsymbol{x}_C}{dt} = \boldsymbol{T}_C^{-1}(\boldsymbol{B}_{11} - \boldsymbol{B}_{12}\boldsymbol{B}_{22}^{-1}\boldsymbol{B}_{21})\boldsymbol{u} + \boldsymbol{T}_C^{-1}(\boldsymbol{b}_1 - \boldsymbol{B}_{12}\boldsymbol{B}_{22}^{-1}\boldsymbol{b}_2)u_D \tag{11}$$

which can be simplified as:

$$\frac{d\boldsymbol{x}_C}{dt} = \boldsymbol{B}_C\boldsymbol{u} + \boldsymbol{b}_D u_D \tag{12}$$

i_S can be represented as a function of $\boldsymbol{x}_C$ as:

$$i_S = \boldsymbol{c}_C\boldsymbol{x}_C \tag{13}$$

where $\boldsymbol{c}_C = \boldsymbol{e}_7^{\mathrm{T}}$. $\boldsymbol{e}_k$ denotes the unit vector with the k-th element equals to 1. The dimension of $\boldsymbol{e}$ is same as the vector dimension of the state variable $\boldsymbol{x}_C$, and the value of k is the position of the extracted state variable in the vector of the state variable.

The state equations of the circuit representation in an interval of rectifier side can be uniformly expressed as:

$$\begin{aligned} \frac{d\boldsymbol{x}_{RC}}{dt} &= \boldsymbol{B}_{RC}^i\boldsymbol{u}_R + \boldsymbol{b}_{RD}^i u_{RD} \\ i_{RS} &= \boldsymbol{c}_{RC}\boldsymbol{x}_{RC} \end{aligned} \tag{14}$$

where the state variables vector $\boldsymbol{x}_{RC}$ consists of the currents. $\boldsymbol{u}_R$ consists of the instantaneous AC system bus voltages of the rectifier side. u_{RD} denotes the instantaneous DC voltage of the rectifier side. $\boldsymbol{B}_{RC}^i$ and $\boldsymbol{b}_{RD}^i$ are the input matrices. The superscript 'i' denotes the i-th operation status. For different conduction and commutation intervals, the equivalent circuit will be different. Accordingly, the matrices need to be reformed.

The equations of inverter side can also be represented as follows:

$$\begin{aligned} \frac{d\boldsymbol{x}_{IC}}{dt} &= \boldsymbol{B}_{IC}^j\boldsymbol{u}_I + \boldsymbol{b}_{ID}^j u_{ID} \\ i_{IS} &= \boldsymbol{c}_{IC}\boldsymbol{x}_{IC} \end{aligned} \tag{15}$$

There are tens of circuit topologies under normal and abnormal operation status. In this part, only one kind of circuit topology is introduced to illustrate the mathematical model of the PES. For different operation status, the differential equations (4)-(6) remain the same. However, the algebraic equations, i.e., (7) and (8), need to be formed according to the change of circuit topology.

B. DC FILTERS AND DC LINE

Similarly, the single-tuned filters of the rectifier and inverter sides have the state-space description of:

$$\begin{aligned} \frac{d\boldsymbol{x}_{RF}}{dt} &= \boldsymbol{A}_{RF}\boldsymbol{x}_{RF} + \boldsymbol{b}_{RF}u_{RD} \\ i_{RF} &= \boldsymbol{c}_{RF}\boldsymbol{x}_{RF} \end{aligned} \tag{16}$$

and:

$$\begin{aligned} \frac{d\boldsymbol{x}_{IF}}{dt} &= \boldsymbol{A}_{IF}\boldsymbol{x}_{IF} + \boldsymbol{b}_{IF}u_{ID} \\ i_{IF} &= \boldsymbol{c}_{IF}\boldsymbol{x}_{IF} \end{aligned} \tag{17}$$

respectively,where $\boldsymbol{x}_{RF} = [u_{RC}\ i_{RF}]^{\mathrm{T}}, \boldsymbol{x}_{IF} = [u_{IC}\ i_{IF}]^{\mathrm{T}}$ and $\boldsymbol{A}_{RF}, \boldsymbol{b}_{RF}, \boldsymbol{c}_{RF}, \boldsymbol{A}_{IF}, \boldsymbol{b}_{IF}, \boldsymbol{c}_{IF}$ are the corresponding coefficient matrices. The inputs u_{RD} and u_{ID} are DC line voltages of the rectifier and inverter sides, respectively.

As depicted in Fig. 4, the state-space representation of the DC lines is described as:

$$\begin{aligned} \frac{d\boldsymbol{x}_D}{dt} &= \boldsymbol{A}_D\boldsymbol{x}_D + \boldsymbol{b}_{D1}u_{RD} + \boldsymbol{b}_{D2}u_{ID} \\ i_{RD} &= \boldsymbol{c}_{D1}\boldsymbol{x}_D \\ i_{ID} &= \boldsymbol{c}_{D2}\boldsymbol{x}_D \end{aligned} \tag{18}$$

where $\boldsymbol{x}_D = [i_{RD},\ i_{ID},\ u_D]^{\mathrm{T}}, \boldsymbol{b}_{D1}$ and $\boldsymbol{b}_{D2}$ are the corresponding coefficient matrices. The output matrices in (18) are $\boldsymbol{c}_{D1} = \boldsymbol{e}_1^{\mathrm{T}}$ and $\boldsymbol{c}_{D2} = \boldsymbol{e}_2^{\mathrm{T}}$. For detail processes of Eqn (16), (17) and (18), please see Appendix B.

C. STATE FUNCTION OF THE PES

PES has the state vector $\bar{\boldsymbol{x}} = [\boldsymbol{x}_{RC}^{\mathrm{T}} \ \boldsymbol{x}_{RF}^{\mathrm{T}} \ \boldsymbol{x}_{D}^{\mathrm{T}} \ \boldsymbol{x}_{IF}^{\mathrm{T}} \ \boldsymbol{x}_{IC}^{\mathrm{T}}]^{\mathrm{T}}$, input vector $\boldsymbol{u} = [\boldsymbol{u}_R^{\mathrm{T}} \ \boldsymbol{u}_I^{\mathrm{T}}]^{\mathrm{T}}$, and algebraic vector $\bar{\boldsymbol{y}} = [u_{RD} \ i_{RS} \ i_{RF} \ i_{RD} \ i_{ID} \ i_{IF} \ i_{IS} \ u_{ID}]^{\mathrm{T}}$. Superscript 'T' denotes the transposition of matrices and vectors.

During the k-th time interval $t \in [t_k^S \ t_k^E]$, where the rectifier and inverter operate on the i-th and j-th operation status respectively, the currents on the rectifier side have the following relationship:

$$i_{RS} - i_{RF} - i_{RD} = 0 \tag{19}$$

Differentiating equation (19) results in $\frac{di_{RS}}{dt} - \frac{di_{RF}}{dt} - \frac{di_{RD}}{dt} = 0$.

Considering (14), (16) and (18), thus:

$$\boldsymbol{k}_{RC}^{i}\boldsymbol{u}_R - \boldsymbol{k}_{RF}\boldsymbol{x}_{RF} - \boldsymbol{k}_{D1}\boldsymbol{x}_D + \bar{k}_R^i u_{RD} - \tilde{k}_R u_{ID} = 0 \tag{20}$$

where $\boldsymbol{k}_{RC}^{i} = \boldsymbol{c}_{RC}\boldsymbol{B}_{RC}^{i}$, $\boldsymbol{k}_{RF} = \boldsymbol{c}_{RF}\boldsymbol{A}_{RF}$, $\boldsymbol{k}_{D1} = \boldsymbol{c}_{D1}\boldsymbol{A}_D$, $\bar{k}_R^i = \boldsymbol{c}_{RC}\boldsymbol{b}_{RD}^{i} - \boldsymbol{c}_{RF}\boldsymbol{b}_{RF} - \boldsymbol{c}_{D1}\boldsymbol{b}_{D1}$ and $\tilde{k}_R = \boldsymbol{c}_{D1}\boldsymbol{b}_{D2}$.

Similarly, the inverter side has the relationship:

$$\boldsymbol{k}_{IC}^{j}\boldsymbol{u}_I - \boldsymbol{k}_{IF}\boldsymbol{x}_{IF} - \boldsymbol{k}_{D2}\boldsymbol{x}_D + \bar{k}_I^j u_{ID} - \tilde{k}_I u_{RD} = 0. \tag{21}$$

where $\boldsymbol{k}_{IC}^{j} = \boldsymbol{c}_{IC}\boldsymbol{B}_{IC}^{j}$, $\boldsymbol{k}_{IF} = \boldsymbol{c}_{IF}\boldsymbol{A}_{IF}$, $\boldsymbol{k}_{I1} = \boldsymbol{c}_{D2}\boldsymbol{A}_D$, $\bar{k}_I^i = \boldsymbol{c}_{IC}\boldsymbol{b}_{ID}^{i} - \boldsymbol{c}_{IF}\boldsymbol{b}_{IF} - \boldsymbol{c}_{D2}\boldsymbol{b}_{D2}$ and $\tilde{k}_I = \boldsymbol{c}_{D2}\boldsymbol{b}_{D2}$.

The state space representation of PES can be formed by substituting (14)-(18), (20) and (21) in (22), as shown at the bottom of the next page, Equation (22) can be written in a compact form as:

$$\begin{aligned} \frac{d\bar{\boldsymbol{x}}}{dt} &= \bar{\boldsymbol{A}}\bar{\boldsymbol{x}} + \bar{\boldsymbol{B}}_1\bar{\boldsymbol{y}} + \bar{\boldsymbol{B}}_2\boldsymbol{u} \\ \boldsymbol{0} &= \bar{\boldsymbol{C}}\bar{\boldsymbol{x}} + \bar{\boldsymbol{D}}_1\bar{\boldsymbol{y}} + \bar{\boldsymbol{D}}_2\boldsymbol{u} \end{aligned} \tag{23}$$

where $\bar{\boldsymbol{x}} = [\boldsymbol{x}_{RC}^{\mathrm{T}} \ \boldsymbol{x}_{RF}^{\mathrm{T}} \ \boldsymbol{x}_{D}^{\mathrm{T}} \ \boldsymbol{x}_{IF}^{\mathrm{T}} \ \boldsymbol{x}_{IC}^{\mathrm{T}}]^{\mathrm{T}}, \boldsymbol{u} = [\boldsymbol{u}_R^{\mathrm{T}} \ \boldsymbol{u}_I^{\mathrm{T}}]^{\mathrm{T}}$. $\bar{\boldsymbol{A}}, \bar{\boldsymbol{B}}_1, \bar{\boldsymbol{B}}_2, \bar{\boldsymbol{C}}, \bar{\boldsymbol{D}}_1$ and $\bar{\boldsymbol{D}}_2$ are the corresponding submatrices. $\bar{\boldsymbol{y}}$ represents the vector of algebraic variables in (22). Eliminating $\bar{\boldsymbol{y}}$ in (23) results in:

$$\frac{d\bar{\boldsymbol{x}}}{dt} = \bar{\boldsymbol{A}}_k\bar{\boldsymbol{x}} + \bar{\boldsymbol{B}}_k\boldsymbol{u} \tag{24}$$

where $\bar{\boldsymbol{A}}_k = \bar{\boldsymbol{A}} - \bar{\boldsymbol{B}}_1\bar{\boldsymbol{D}}_1^{-1}\bar{\boldsymbol{C}}$, $\bar{\boldsymbol{B}}_k = \bar{\boldsymbol{B}}_2 - \bar{\boldsymbol{B}}_1\bar{\boldsymbol{D}}_1^{-1}\bar{\boldsymbol{D}}_2$. The Subscript '$k$' denotes the k-th time interval.

D. MODEL SIMPLIFICATION

The instantaneous AC bus voltages have the form:

$$\boldsymbol{u}_R = \begin{bmatrix} U_{RA}\cos(\omega t + \theta_{RA}) \\ U_{RB}\cos(\omega t + \theta_{RB}) \\ U_{RC}\cos(\omega t + \theta_{RC}) \end{bmatrix}$$

and

$$\boldsymbol{u}_I = \begin{bmatrix} U_{IA}\cos(\omega t + \theta_{IA}) \\ U_{IB}\cos(\omega t + \theta_{IB}) \\ U_{IC}\cos(\omega t + \theta_{IC}) \end{bmatrix}.$$

Introduce virtual variables $\boldsymbol{v}_R$ and $\boldsymbol{v}_I$, where:

$$\boldsymbol{v}_R = \begin{bmatrix} U_{RA}\sin(\omega t + \theta_{RA}) \\ U_{RB}\sin(\omega t + \theta_{RB}) \\ U_{RC}\sin(\omega t + \theta_{RC}) \end{bmatrix}$$

and

$$\boldsymbol{v}_I = \begin{bmatrix} U_{IA}\sin(\omega t + \theta_{IA}) \\ U_{IB}\sin(\omega t + \theta_{IB}) \\ U_{IC}\sin(\omega t + \theta_{IC}) \end{bmatrix}.$$

Therefore, $\frac{d\boldsymbol{u}}{dt} = -\omega\boldsymbol{v}$, $\frac{d\boldsymbol{v}}{dt} = \omega\boldsymbol{u}$, where $\boldsymbol{v} = [\boldsymbol{v}_R^{\mathrm{T}} \ \boldsymbol{v}_I^{\mathrm{T}}]$. Thus, taking into account (24), the following equation can be provided:

$$\frac{d}{dt}\begin{bmatrix} \bar{\boldsymbol{x}} \\ \boldsymbol{u} \\ \boldsymbol{v} \end{bmatrix} = \begin{bmatrix} \bar{\boldsymbol{A}}_k & \bar{\boldsymbol{B}}_k & \\ & & -\omega\boldsymbol{I}_6 \\ & \omega\boldsymbol{I}_6 & \end{bmatrix}\begin{bmatrix} \bar{\boldsymbol{x}} \\ \boldsymbol{u} \\ \boldsymbol{v} \end{bmatrix} \tag{25}$$

where $\boldsymbol{I}_n$ is an n-by-n identity matrix. (25) can be written in a short form as:

$$\frac{d\boldsymbol{x}}{dt} = \boldsymbol{A}_k\boldsymbol{x} \tag{26}$$

Consequently, the non-homogeneous linear differential (24) is simplified to a homogeneous linear differential equation given in (26).

The DC currents i_{RS} and i_{IS}, and DC line voltage u_D can be represented as:

$$\boldsymbol{w} = \boldsymbol{C}_k\boldsymbol{x} \tag{27}$$

where $\boldsymbol{w} = [i_{RS} \ u_D \ i_{IS}]^{\mathrm{T}}$. $\boldsymbol{w}$ is sent to CS to generate the firing angles.

As the operation status of the rectifier or inverter changes, the equivalent circuit will be different. Although the state vector for each operation status is identical, it requires reformulating $\boldsymbol{A}_k$ for a different system operation status. The definition of time intervals will be described in the next subsection.

E. ANALYTICAL SOLUTION OF PES

Suppose that the state variable has the initial value $\boldsymbol{x}_k^S$ at the beginning of the k-th time interval. The time-domain response of the PES in this interval can be expressed as:

$$\boldsymbol{x} = e^{\boldsymbol{A}_k(t - t_k^S)}\boldsymbol{x}_k^S \tag{28}$$

where $e^{\boldsymbol{A}_k t}$ is the exponential matrix and $t \in [t_k^S, t_k^E]$. t_k^S and t_k^E are the start and end moments of this time interval, respectively, which are determined by the triggering time controlled by CS and the end time of the commutation interval.

When the $k+1$-th time interval begins, the state vector cannot mutate. Therefore:

$$\boldsymbol{x}_{k+1}^S = \boldsymbol{x}_k^E \tag{29}$$

F. VALVES FIRING PULSE AND TIME INTERVALS OF PES

In the equidistant pulse control logic, the reference phase will be generated at an interval of $\pi/6$. After each reference phase, CS generates firing pulses after delay angles α and $\pi - \beta$ for the rectifier and inverter side converters, respectively. Taking a period of steady state as an example, the statuses of all converters are shown in Fig. 6. Where θ_{PR} and θ_{PI} are the output angles of the phase-locked loop (PLL)

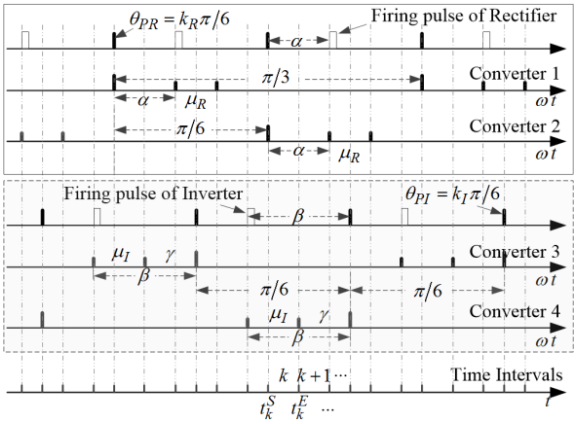

FIGURE 6. Firing pulse and time intervals of the PES.

in rectifier and inverter side, respectively; and μ_R and μ_I are the respective rectifier and inverter overlap angles. For a different converter status, the equivalent circuit of PES needs to be updated. Consequently, the time intervals in PES will be formed taking into account the status of each converter in the rectifier and inverter sides. Moreover, the overlap angle and extinction angle need to be computed.

G. CALCULATION OF THE OVERLAP ANGLE AND EXTINCTION ANGLE

The overlap angle μ is not explicitly contained in the state and algebraic variables. It is associated with the commutation angle of the inverter and the zero crossing of the line voltages. Thus, it needs to be computed.

Assuming the k-th operation status is the commutation status, the commutation current $i_c(t)$ can be calculated as:

$$i_c(t) = \boldsymbol{a}_k^{\mathrm{T}}\boldsymbol{x}(t) \tag{30}$$

where $\boldsymbol{a}_k^{\mathrm{T}}$ is a coefficient vector. At the turn-on time of the commutation interval t_k^S, the commutation current $i_c(t_k^S)$ is greater than zero. The turn-off time t_k^E can be derived by checking the commutation current $i_c(t) = 0$, i.e.:

$$i_c(t_k^E) = \boldsymbol{a}_k^{\mathrm{T}} e^{\boldsymbol{A}_k(t_k^E - t_k^S)}\boldsymbol{x}(t_k^S) = 0. \tag{31}$$

Thus, the turn-off time t_k^E can be obtained by solving (31) using Newton's or secant methods. The overlap angle μ is calculated as:

$$\mu = 2\pi(t_k^E - t_k^S)\Big/T \tag{32}$$

where T is a cycle of the AC system. Consequently, the extinction angle γ can be obtained by:

$$\gamma = \beta - \mu \tag{33}$$

H. CALCULATION OF FUNDAMENTAL AND HARMONIC COMPONENTS

For the simulation of AC systems, the fundamental components are needed. They can be derived by Fourier decomposition, which is expressed as:

$$\boldsymbol{x}(t) = \frac{\boldsymbol{a}_0}{2} + \sum_{n=1}^{\infty} \boldsymbol{a}_n \cos(n\omega t) + \boldsymbol{b}_n \sin(n\omega t) \tag{34}$$

The analytical solution of the fundamental component and n-th harmonics of $\boldsymbol{x}(t)$ also exists. It can be computed by:

$$\begin{aligned}\boldsymbol{a}_n - \mathrm{j}\boldsymbol{b}_n &= \frac{2}{T}\int_0^T e^{-\mathrm{j}n\omega t}\boldsymbol{x}(t)dt \\ &= \frac{2}{T}\sum_{k=1}^{N}\int_{t_k^S}^{t_k^E} e^{-\mathrm{j}n\omega t} e^{\boldsymbol{A}_k(t-t_k^S)}\boldsymbol{x}(t_k^S)dt \\ &= \frac{2}{T}\sum_{k=1}^{N}\int_0^{t_k^E - t_k^S} e^{(-\mathrm{j}n\omega\boldsymbol{I}+\boldsymbol{A}_k)t}dt\,(e^{-\mathrm{j}n\omega t_k^S}\boldsymbol{x}_k^S)\end{aligned} \tag{35}$$

where N is the number of operation status in an AC cycle.

V. MODELLING AND SIMULATION OF THE CS

For different HVDC systems, the CS may have different control logics. In this section, the Cigre HVDC benchmark system is selected as an example [17].

$$\frac{d}{dt}\begin{bmatrix}\boldsymbol{x}_{RC}\\ \boldsymbol{x}_{RF}\\ \boldsymbol{x}_D\\ \boldsymbol{x}_{IF}\\ \boldsymbol{x}_{IC}\\ \hline 0\\ 0\\ 0\\ 0\\ 0\\ 0\\ 0\\ 0\end{bmatrix} = \left[\begin{array}{ccccc:cccccccc} & \boldsymbol{A}_{RF} & & & & \boldsymbol{b}_{RD}^i & & & & & & \boldsymbol{b}_{D2} & \\ & & \boldsymbol{A}_D & & & \boldsymbol{b}_{RF} & & & & & & \boldsymbol{b}_{IF} & \\ & & & \boldsymbol{A}_{IF} & & \boldsymbol{b}_{D1} & & & & & & \boldsymbol{b}_{ID}^j & \\ \hline \boldsymbol{c}_{RC} & & & & & & -1 & & & & & & \\ & \boldsymbol{c}_{RF} & & & & & & -1 & & & & & \\ & & \boldsymbol{c}_{D1} & & & & & & -1 & & & & \\ & & \boldsymbol{c}_{D2} & & & & & & & -1 & & & \\ & & & \boldsymbol{c}_{IF} & & & & & & & -1 & & \\ & & & & \boldsymbol{c}_{IC} & & & & & & & -1 & \\ & -\boldsymbol{k}_{RF} & -\boldsymbol{k}_{D1} & & & \bar{k}_R^i & & & & & & -\tilde{k}_R & \\ & & -\boldsymbol{k}_{D2} & -\boldsymbol{k}_{IF} & & -\tilde{k}_I & & & & & & \bar{k}_I^j & \end{array}\right]\begin{bmatrix}\boldsymbol{x}_{RC}\\ \boldsymbol{x}_{RF}\\ \boldsymbol{x}_D\\ \boldsymbol{x}_{IF}\\ \boldsymbol{x}_{IC}\\ \hline u_{RD}\\ i_{RS}\\ i_{RF}\\ i_{RD}\\ i_{ID}\\ i_{IF}\\ i_{IS}\\ u_{ID}\end{bmatrix} + \left[\begin{array}{cc} \boldsymbol{B}_{RC}^i & \\ & \\ & \boldsymbol{B}_{IC}^j \\ \hline & \\ & \\ & \\ & \\ & \\ & \\ & \\ \boldsymbol{k}_{RC}^i & \\ & \boldsymbol{k}_{IC}^j \end{array}\right]\begin{bmatrix}\boldsymbol{u}_R\\ \boldsymbol{u}_I\end{bmatrix} \tag{22}$$

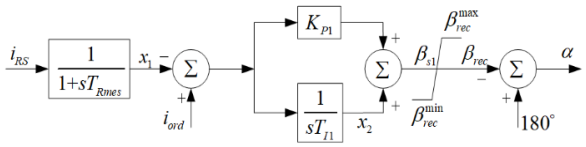

FIGURE 7. Block diagram of rectifier control system.

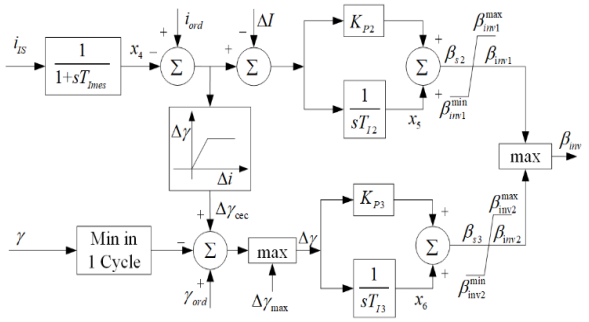

FIGURE 8. Block diagram of inverter control system.

A. CS OF HVDC SYSTEM

The rectifier of the Cigre HVDC system adopts constant current control and the inverter adopts constant current and extinction angle control. The block diagrams of the controllers are shown in Fig. 7 and Fig. 8, where i_{RS} and i_{IS} denote the DC current of the rectifier and inverter sides, respectively. The control system generates the delay angle α and the advance angle β for the rectifier and inverter, respectively. γ in Fig. 8 is the extinction angle.

In Fig. 7 and Fig. 8, the limited current reference i_{ord} is generated by means of the Voltage Dependent Current Limit (VDCL) unit, as shown in Fig. 9.

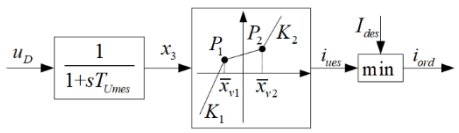

FIGURE 9. Block diagram of VDCL.

The model of CS is described by nonlinear differential and algebraic functions since there are nonlinear items in the diagrams, such as limiters and the piecewise function:

$$\begin{aligned} \dot{\boldsymbol{y}} &= \boldsymbol{f}(\boldsymbol{y},\ \boldsymbol{z},\ \boldsymbol{w}) \\ \boldsymbol{0} &= \boldsymbol{g}(\boldsymbol{y},\ \boldsymbol{z}) \end{aligned} \tag{36}$$

where $\boldsymbol{y} = [x_1\ \ x_2\ \ x_3\ \ x_4\ \ x_5\ \ x_6]^{\mathrm{T}}$ and $\boldsymbol{z} = [\beta_{s1}\ \ \beta_{rec}\ \ \alpha\ \ \Delta\gamma_{cec}\ \ \Delta\gamma\ \ \beta_{s2}\ \ \beta_{inv1}\ \ \beta_{s3}\ \ \beta_{inv2}\ \ \beta_{inv}\ \ I_{use}]^{\mathrm{T}}$, which are the state variables and algebraic variables of CS, respectively. $\boldsymbol{w} = [I_{RS}\ \ u_D\ \ I_{IS}\ \ \gamma]^{\mathrm{T}}$ is input obtained from the PES. The detail description of Eqn.(36) is represented in Appendix C for saving spaces.

In addition, the logic of PLL [18], available in the valve control layer, is shown in Fig. 10, where u_a, u_b and u_c are

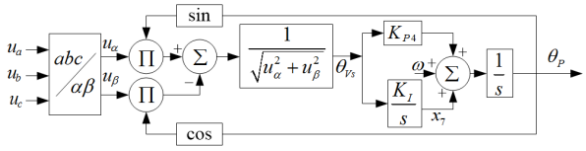

FIGURE 10. Block diagram of PLL.

instantaneous values of three-phase voltages. The output θ_P is applied to generate the firing pulse.

B. SIMULATION OF CS

Since the control system is nonlinear, the numerical method is better to be adopted for the simulation purposes. Furthermore, the Backward Euler method is adopted to avoid numerical oscillations [19].

Applying backward Euler method to (36) results in:

$$\begin{aligned} \boldsymbol{y}(t+\Delta t) &= \boldsymbol{y}(t) + \boldsymbol{f}(\boldsymbol{y}(t+\Delta t),\ \boldsymbol{z}(t+\Delta t),\ \boldsymbol{w}(t+\Delta t)) \\ \boldsymbol{0} &= \boldsymbol{g}(\boldsymbol{y}(t+\Delta t),\ \boldsymbol{z}(t+\Delta t)) \end{aligned} \tag{37}$$

where Δt represents the integral step. As $\boldsymbol{w}(t+\Delta t)$ obtained from simulation of PES, $\boldsymbol{y}(t+\Delta t)$ and $\boldsymbol{z}(t+\Delta t)$ can be computed by solving (37).

C. INTEGRAL STEPS OF CS SIMULATION

Comparing with the behavior of PES, the transient process of CS is much slower. Thus, a large simulation step length can be adopted. Considering that time-interval of each operation status is different in the transient simulation of PES, a variable step-size can be adopted in the simulation of CS. As the time-interval of a PES operation status is derived, the step-length of CS changes accordingly. That is, the calculated time-interval of the PES operation status is adopted for simulating CS. The simulation of PES and CS is interchangeably processed. It's worth mentioning that the maximum period of PES is only a few milliseconds for the purposes of transient simulations, which is enough for the numerical simulation of CS.

VI. STEADY STATE VALUE AND PROCEDURE

The transient simulation starts from a steady state. This section discusses the computation of steady state, followed by an illustration of a transient simulation procedure.

A. COMPUTING THE STEADY STATE OF HVDC

Given three phase voltages of both rectifier and inverter sides and the control references I_{des} and γ_{ord}, the steady state result is utilized to determine α, β and the corresponding states of the PES and CS systems at a specific time t_0. The steady state of the HVDC system is periodic. That is, the steady state needs to satisfy the condition:

$$\left\| \begin{matrix} \boldsymbol{x}(t_0+T) - \boldsymbol{x}(t_0) \\ \boldsymbol{y}(t_0+T) - \boldsymbol{y}(t_0) \end{matrix} \right\| < \varepsilon \tag{38}$$

where T is the period of the AC voltage and ε is a tolerance.

Consider that $\boldsymbol{x}$ and $\boldsymbol{y}$ satisfy (26) and(38). In an AC cycle, they change with respect to t. Furthermore, the time intervals

of PES need to be determined by calculation. Hence, it is almost impossible to directly calculate $\boldsymbol{x}(t_0)$ and $\boldsymbol{y}(t_0)$. In this section, the iterative simulation is utilized to calculate the steady state. The initial values of $\alpha, \beta, \boldsymbol{x}$ and $\boldsymbol{y}$ at t_0 can be calculated using quasi-steady state model [4].

The procedure for computing the steady state of the HVDC system is as follows:

Step 1: Input the three-phase AC system voltages, the controller references and a tolerance ε.

Step 2: Calculate the initial values of α, β, $\boldsymbol{x}(t_0)$ and $\boldsymbol{y}(t_0)$ by quasi-steady state model.

Step 3: Set $t = t_0$. Perform the following procedure until (38) is satisfied.

> **Step 3.1:** Identify the current operation status of PES. Formulate the state matrix and compute the response by (28). Determine the end time of the operation status as shown in section IV.G. Compute the time interval Δt of the operation status.
>
> **Step 3.2:** Set the simulation step as Δt. Calculate the transient response of CS by Backward Euler method, as described in section V.B.
>
> **Step 3.3:** Set $t = \min(t + \Delta t, t_0 + T)$. If $t \neq t_0 + T$, go to step 3.1. Otherwise, compute $\boldsymbol{x}(t)$ and $\boldsymbol{y}(t)$.
>
> **Step 3.4:** If the condition (38) is not satisfied, set $t = t_0 + T, \boldsymbol{x}(t_0) = \boldsymbol{x}(t)$ and $\boldsymbol{y}(t_0) = \boldsymbol{y}(t)$; then go to step 3.1. Otherwise, terminate the loop. The initial value of the steady state at t_0 is obtained as $\boldsymbol{x}(t)$ and $\boldsymbol{y}(t)$.

B. SIMULATION OF TRANSIENT RESPONSE

In transient simulations, the amplitudes and phases of AC voltages may fluctuate. Consequently, it only needs to perform steps 3.1 and 3.2 to calculate the transient response. In this case, the AC voltages are derived by AC system simulation. The operation status of the PES needs to be identified step by step according to the simulation result due to the possibility of commutation failures.

VII. NUMERICAL RESULTS

A uni-polar 12-pulse CIGRE benchmark system is used as the testing system. According to the assumptions listed in section II, the AC filters and equivalent impedance of the AC system are ignored. In addition, the DC filters are equipped on both sides of the DC lines. In the following simulations, the frequency of the AC system is set as 50Hz. The parameters of both DC filters are $L = 70.4$mH, $C = 10\mu F$ and $R = 5.3\Omega$. The parameters of other elements are the same as the CIGRE benchmark system [17].

The accuracy and efficiency of the proposed method are verified by comparing the simulation results produced by the proposed method, which is realized in MATLAB codes, with that simulated by PSCAD software packages. Both symmetric and asymmetric AC voltages are applied during the simulation of the transient response. The effective values of line voltages of the rectifier and inverter sides are 345kV and 226.55kV, respectively. The rectifier of the Cigre HVDC system adopts constant current control and the inverter adopts constant current and extinction angle control. The constant current value is 2kA and the extinction angle is 15°.

A. SIMULATION OF STEADY-STATE RESPONSE

The delay angle α and advance angle β, obtained by the proposed method and PSCAD software packages are shown in Table 1. Obviously, the calculation results of the angle α and β are almost the same.

TABLE 1. Calculation result of delay angle and advance angle.

	The proposed method	PSCAD/EMTDC	Error
α	14.61°	14.92°	0.31°
β	37.87°	37.80°	0.07°

The DC voltage and DC current of the inverter side and the rectifier side in half a cycle are shown in Fig. 11.

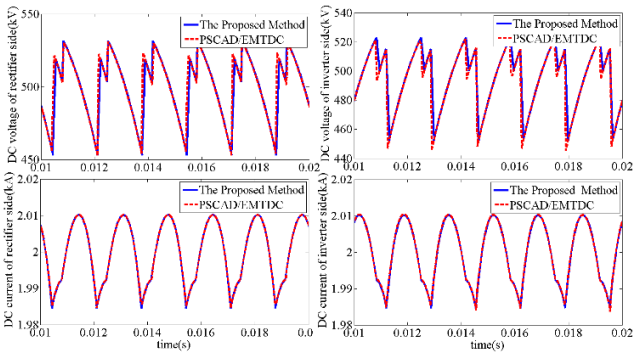

FIGURE 11. The DC voltage and DC current of the inverter and the rectifier side in half a cycle under steady-state operation.

As observed in Fig. 11, the results computed by the proposed method are same as the ones generated using PSCAD/EMTDC. The fundamental and harmonic components of the AC bus current in the rectifier and inverter sides are listed in Table 2. It shows that the current components obtained by the proposed method and PSCAD/EMTDC are almost the same.

TABLE 2. Fundamental and harmonic components of the AC bus current in the rectifier and inverter sides.

	Fundamental		11^{th} harmonic		13^{th} harmonic	
	Proposed method	PSCAD/EMTDC	Proposed method	PSCAD/EMTDC	Proposed method	PSCAD/EMTDC
I_R (kA)	1.9086	1.9063	0.0629	0.0630	0.0382	0.0381
I_I (kA)	2.8630	2.8600	0.0950	0.0956	0.0579	0.0581

B. TRANSIENT SIMULATION WITH SYMMETRIC AND ASYMMETRIC VARIATION OF AC VOLTAGE

The transient simulation of the HVDC system response is tested under symmetric and asymmetric AC system faults. For the cases, only the variation of AC voltages in the inverter side bus is considered.

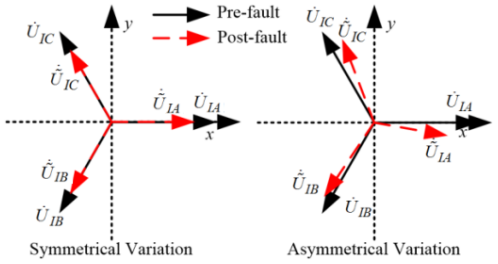

FIGURE 12. AC system voltage after symmetric and asymmetric faults.

TABLE 3. Effective value of AC system phase voltage after symmetric and asymmetric faults.

	Pre-fault	Symmetric AC fault of inverter side	Asymmetric AC fault of inverter side
Phase A(kV)	$131\angle 0^\circ$	$117.9\angle 0^\circ$	$92.7\angle -10^\circ$
Phase B(kV)	$131\angle 240^\circ$	$117.9\angle 240^\circ$	$113.0\angle 236^\circ$
Phase C(kV)	$131\angle 120^\circ$	$117.9\angle 120^\circ$	$112.8\angle 111^\circ$

The pre-fault and post-fault AC voltages adopted in this paper are shown in Fig. 12 and Table 3. Both faults happen at 1.0s and the voltages recover after 0.1s. For the symmetric case, the inverter side voltage drops to a value of 0.90 times the pre-fault case. For asymmetric case, the variation happens in the voltage amplitudes and phase angles.

The waveforms under the symmetric and asymmetric disturbances are shown in Fig. 13 and Fig. 14, respectively. As it can be observed from the figures, the results computed by the proposed method are almost the same as those obtained by PSCAD/EMTDC.

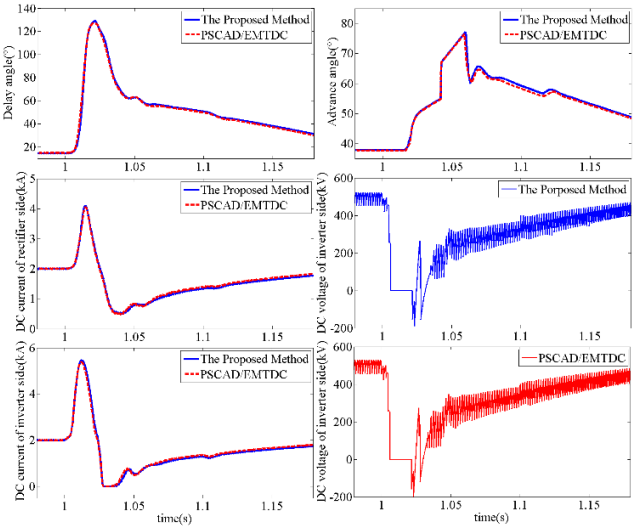

FIGURE 13. Waveforms under symmetric disturbance.

The minimum extinction angles in one cycle computed by the proposed method and PSCAD/EMTDC under symmetric and asymmetric AC fault are shown in Fig. 15. Counting from

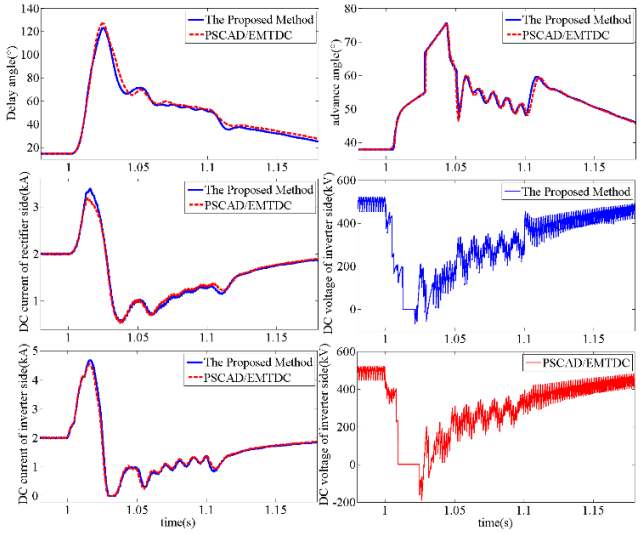

FIGURE 14. Waveforms under asymmetric disturbance.

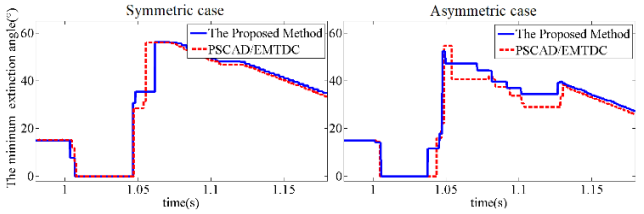

FIGURE 15. The minimum extinction angle in one cycle.

the time the fault began, in symmetric case, both the proposed method and PSCAD/EMTDC capture the first commutation failure in the third commutation status process. In asymmetric case, both methods capture the first commutation failure in the second commutation process.

C. COMPUTATIONAL PERFORMANCE ANALYSIS

In the steady state simulation, the deviation of the advance angle, obtained by the proposed method and PSCAD/EMTDC, is only 0.07°. There is oscillation of the DC voltage in PSCAD result, but the DC voltage is steady in proposed method. Which are shown in Fig.16. In the transient simulation, the maximum deviation is 0.40°.

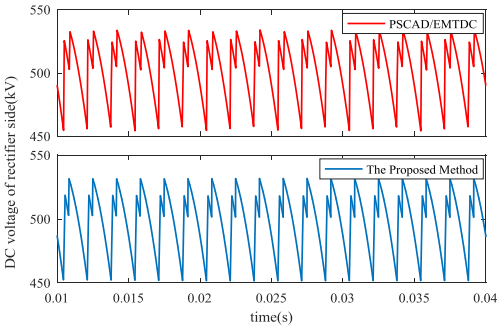

FIGURE 16. The state DC voltage of rectifier side.

There are several reasons this mismatch may occur. First, the truncation error is an inherited problem of the numerical integration, which would cause errors even numerical oscillations to the result of PSCAD/EMTDC. That is the reason of the oscillation in the PSCAD result in Fig. 16. Second, the extinction angle calculated in PSCAD/EMTDC using the interpolation method is a little bit different from that calculated by the proposed method applying the analytical method. Third, the simulations of PES and CS using the proposed method are interchangeably executed with a variable step-size. In contrast, PES and CS are simultaneously simulated in PSCAD/EMTDC with a fixed step size.

The proposed method also provides a faster computational speed compared with the simulation results produced by PSCAD/EMTDC. It requires a CPU time of about 10.43s to simulate 100 AC periods while it needs 12.69s for PSCAD/EMTDC (with a time-step of 50μs).

VIII. CONCLUSION

A new method for simulating the transient response of HVDCs in the hybrid electro-mechanical and electromagnetic systems is proposed. The boundaries for hybrid simulation as well as the interface for electromagnetic simulation of HVDC, the state-space representation and transient process simulation are introduced.

The HVDC system in our model is described as PES and CS. According to appropriate assumptions, in different operation status, the PES is described as linear homogeneous differential equations. The analytical solution of this part is derived. The CS is formulated as nonlinear differential-algebraic equations. We use numerical integration method with a variable step length to compute the response. The PES and CS are calculated alternatively to obtain the dynamic behavior of HVDC.

Theoretically, since the analytical method is adopted, the proposed method performs better in accuracy. In numerical tests, the results of the proposed method and PSCAD/EMTDC are consistent with each other. Moreover, the proposed method is a little faster in computational time.

APPENDIX

A. DETAILED CONTENTS OF MATRICES IN EQN.(10)

$$\boldsymbol{B}_{11} = \begin{bmatrix} k_y & & \\ & k_y & \\ & & k_y \\ \hdashline k_d & & \\ & k_d & \\ & & k_d \\ \hdashline & & \end{bmatrix}_{7\times 3}$$

$$\boldsymbol{B}_{12} = \begin{bmatrix} -1 & & & & & & & \\ & -1 & & & & & & \\ & & -1 & & & & & \\ \hdashline & & & -1 & & & & \\ & & & & -1 & & & \\ & & & & & -1 & & \\ \hdashline & & & & & & 1 & 1 \end{bmatrix}_{7\times 8}$$

$$\boldsymbol{B}_{21} = \begin{bmatrix} k_y & k_y & k_y \\ & & \\ & & \\ & & \\ -k_y & & \\ \hdashline & k_d & -k_d \\ & & \\ -k_d & & k_d \end{bmatrix}_{8\times 3}$$

$$\boldsymbol{B}_{22} = \begin{bmatrix} -1 & -1 & -1 & & & & & \\ & & & 1 & 1 & 1 & & \\ \hdashline & 1 & -1 & & & & & \\ 1 & -1 & & & & & -1 & \\ 1 & & & & & & K_1 & K_1 \\ \hdashline & & & & -1 & 1 & & \\ & & & 1 & & & & -1 \\ & & & 1 & & -1 & K_2 & K_2 \end{bmatrix}_{8\times 8}$$

$$\boldsymbol{T}_C = \begin{bmatrix} L_y & & & & & & \\ & L_y & & & & & \\ & & L_y & & & & \\ \hdashline & & & L_d & & & \\ & & & & L_d & & \\ & & & & & L_d & \\ \hdashline & & & & & & L_s \end{bmatrix}_{7\times 7}$$

$$\boldsymbol{b}_1 = \begin{bmatrix} \\ \\ \\ \hdashline \\ \\ \hdashline -1 \end{bmatrix}_{7\times 1} \qquad \boldsymbol{b}_2 = \begin{bmatrix} \\ \\ \\ \hdashline \\ -K_1 \\ \hdashline \\ -K_2 \end{bmatrix}_{8\times 1}$$

where $K_1 = L_y/L_S$, $K_2 = L_d/L_S$.

B. DETAIL PROCESS OF EQN(16), (17) AND (18)

The Eqn (16) (rectifier side)and Eqn (17) (inverter side) have the same derivation process. Taking Eqn (16) as an example, the state-space description of the rectifier single-tuned filters shown in Fig. 4 is as follows:

$$\begin{aligned} C_{RF}\frac{du_{RC}}{dt} &= i_{RF} \\ L_{RF}\frac{di_{RF}}{dt} &= u_{RD} - u_{RC} - R_{RF}i_{RF} \end{aligned} \tag{39}$$

which can be written in a compart form as:

$$\boldsymbol{T}\frac{d\boldsymbol{x}_{RF}}{dt} = \bar{\boldsymbol{A}}_{RF}\boldsymbol{x}_{RF} + \bar{\boldsymbol{b}}_{RF}u_{RD} \tag{40}$$

where $\boldsymbol{x}_{RF} = [u_{RC}\ \ i_{RF}]^{\mathrm{T}}, \boldsymbol{T} = \mathrm{diag}(C_{RF},\ L_{RF}), \bar{\boldsymbol{A}}_{RF} = \begin{bmatrix} & 1 \\ -1 & -R_{RF} \end{bmatrix}, \bar{\boldsymbol{b}}_{RF} = \begin{bmatrix} \\ 1 \end{bmatrix}$.

Pre-multiply $\boldsymbol{T}^{-1}$ to(40), the following equation can be obtained:

$$\frac{d\boldsymbol{x}_{RF}}{dt} = \boldsymbol{A}_{RF}\boldsymbol{x}_{RF} + \boldsymbol{b}_{RF}u_{RD} \tag{41}$$

where $\boldsymbol{A}_{RF} = \boldsymbol{T}^{-1}\bar{\boldsymbol{A}}_{RF}$ and $\boldsymbol{b}_{RF} = \boldsymbol{T}^{-1}\bar{\boldsymbol{b}}_{RF}$, the current i_{RF} can be represented as:

$$i_{RF} = \boldsymbol{c}_{RF}\boldsymbol{x}_{RF} \tag{42}$$

where $\boldsymbol{c}_{RF} = \boldsymbol{e}_2^{\mathrm{T}}$. The state space representation of the inverter DC filter (Eqn (17)) can be obtained accordingly.

For Eqn (18), the state-space description of the DC line is as follows:

$$\begin{aligned} L_D\frac{di_{RD}}{dt} &= -R_D i_{RD} - u_D + u_{RD} \\ L_D\frac{di_{ID}}{dt} &= -R_D i_{ID} - u_D + u_{ID} \\ C_D\frac{du_D}{dt} &= i_{RD} + i_{ID} \end{aligned} \tag{43}$$

which can be written in a compart form as:

$$\boldsymbol{T}\frac{d\boldsymbol{x}_D}{dt} = \bar{\boldsymbol{A}}_D\boldsymbol{x}_D + \bar{\boldsymbol{b}}_{D1}u_{RD} + \bar{\boldsymbol{b}}_{D2}u_{ID} \tag{44}$$

where

$\boldsymbol{x}_D = [i_{RD},\ i_{ID},\ u_D]^{\mathrm{T}}, \boldsymbol{T} = diag(L_D,\ L_D,\ C_D)$,

$\bar{\boldsymbol{A}}_D = \begin{bmatrix} -R_D & & -1 \\ & -R_D & -1 \\ 1 & 1 & \end{bmatrix}, \bar{\boldsymbol{b}}_{D1} = \begin{bmatrix} \\ 1 \\ \end{bmatrix}, \bar{\boldsymbol{b}}_{D2} = \begin{bmatrix} 1 \\ \\ \end{bmatrix}$.

Pre-multiply $\boldsymbol{T}^{-1}$ to (44), the following equation can be obtain:

$$\frac{d\boldsymbol{x}_D}{dt} = \boldsymbol{A}_D\boldsymbol{x}_D + \boldsymbol{b}_{D1}u_{RD} + \boldsymbol{b}_{D2}u_{ID} \tag{45}$$

where $\boldsymbol{A}_D = \boldsymbol{T}^{-1}\bar{\boldsymbol{A}}_D$, $\boldsymbol{b}_{D1} = \boldsymbol{T}^{-1}\bar{\boldsymbol{b}}_{D1}$ and $\boldsymbol{b}_{D2} = \boldsymbol{T}^{-1}\bar{\boldsymbol{b}}_{D2}$, the current i_{RD} and i_{ID} can be represented as:

$$\begin{aligned} i_{RD} &= \boldsymbol{c}_{D1}\boldsymbol{x}_D \\ i_{ID} &= \boldsymbol{c}_{D2}\boldsymbol{x}_D \end{aligned} \tag{46}$$

where $\boldsymbol{c}_{D1} = \boldsymbol{e}_1^{\mathrm{T}}, \boldsymbol{c}_{D2} = e_2^{\mathrm{T}}$.

C. DETAIL MATHEMATICAL EXPRESSION OF CS

For the rectifier control system, it can be expressed as:

$$\begin{aligned} T_{Rmes}\frac{dx_1}{dt} &= I_{RS} - x_1 \\ T_{I1}\frac{dx_2}{dt} &= I_{ord} - x_1 \\ \beta_{s1} &= K_{P1}\left[I_{ord} - x_1\right] + x_2 \\ \beta_{rec} &= \mathrm{limited}\{\beta_{rec}^{\max}, \beta_{s1}, \beta_{rec}^{\min}\} \\ \alpha &= \pi - \beta_{rec} \end{aligned} \tag{47}$$

For the inverter control system, it can be expressed as:

$$\begin{aligned} T_{Imes}\frac{dx_4}{dt} &= I_{IS} - x_4 \\ T_{I2}\frac{dx_5}{dt} &= I_{ord} - x_4 - \Delta I \\ T_{I3}\frac{dx_6}{dt} &= \Delta\gamma \\ \Delta\gamma_{cec} &= \begin{cases} 0, & I_{ord} - x_4 \le 0 \\ \frac{\bar{\gamma}_c}{\bar{x}_c}(I_{ord} - x_4), & 0 < I_{ord} - x_4 \le \bar{x}_c \\ \bar{\gamma}_c, & \bar{x}_c < I_{ord} - x_4 \end{cases} \\ \Delta\gamma &= \max\{\Delta\gamma_{\max}, \gamma_{ord} + \Delta\gamma_{cec} - \gamma_{\min}\} \\ \beta_{s2} &= K_{P2}\left[I_{ord} - x_4 - \Delta I\right] + x_5 \\ \beta_{inv1} &= \mathrm{limited}\{\beta_{inv1}^{\max}, \beta_{s2}, \beta_{inv1}^{\min}\} \\ \beta_{s3} &= K_{P3}\Delta\gamma + x_6 \\ \beta_{inv2} &= \mathrm{limited}\{\beta_{inv2}^{\max}, \beta_{s3}, \beta_{inv2}^{\min}\} \\ \beta_{inv} &= \max\{\beta_{inv1}, \beta_{inv2}\} \end{aligned} \tag{48}$$

The function limited$\{\beta^{\max}, \beta, \beta^{\min}\}$ is as follows,

$$\mathrm{limited}\{\beta^{\max}, \beta, \beta^{\min}\} = \begin{cases} \beta^{\max}, & \beta > \beta^{\min} \\ \beta, & \beta^{\min} \le \beta \le \beta^{\max} \\ \beta^{\min}, & \beta < \beta^{\min} \end{cases} \tag{49}$$

For VDCL, it can be expressed as:

$$\begin{aligned} T_{Umes}\frac{dx_3}{dt} &= u_D - x_3 \\ I_{ues} &= \begin{cases} K_1(x_3 - \bar{x}_{v1}) + P_1, & x_3 \le \bar{x}_{v1} \\ K_{12}(x_3 - \bar{x}_{v1}) + P_1, & \bar{x}_{v1} < x_3 \le \bar{x}_{v2} \\ K_2(x_3 - \bar{x}_{v2}) + P_2, & \bar{x}_{v2} < x_3 \end{cases} \\ I_{ord} &= \min\{I_{ues}, I_{des}\} \end{aligned} \tag{50}$$

Apparently, the rectifier and inverter control system together with VDCL can described in a compact form as:

$$\begin{aligned} \dot{\boldsymbol{y}} &= \boldsymbol{f}(\boldsymbol{y}, \boldsymbol{z}, \boldsymbol{w}) \\ \boldsymbol{0} &= \boldsymbol{g}(\boldsymbol{y}, \boldsymbol{z}) \end{aligned} \tag{51}$$

where $\boldsymbol{y} = [x_1\ \ x_2\ \ x_3\ \ x_4\ \ x_5\ \ x_6]^{\mathrm{T}}$ and $\boldsymbol{z} = [\beta_{s1}\ \ \beta_{rec}\ \ \alpha\ \ \Delta\gamma_{cec}\ \ \Delta\gamma\ \ \beta_{s2}\ \ \beta_{inv1}\ \ \beta_{s3}\ \ \beta_{inv2}\ \ \beta_{inv}\ \ I_{use}]^{\mathrm{T}}$, $\boldsymbol{w} = [I_{RS}\ u_D\ I_{IS}\ \gamma]^{\mathrm{T}}$.

The differential-algebraic equations of PLL can be expressed as:

$$\begin{aligned} \frac{dx_7}{dt} &= K_I\theta_{Vs} \\ \frac{d\theta_P}{dt} &= K_{P4}\theta_{Vs} + x_7 + \omega \\ u_\alpha &= \frac{2}{3}u_a - \frac{1}{3}u_b - \frac{1}{3}u_c \\ u_\beta &= \frac{\sqrt{3}}{3}u_b - \frac{\sqrt{3}}{3}u_c \\ \theta_{Vs} &= \frac{1}{\sqrt{u_\alpha^2 + u_\beta^2}}[u_\alpha \sin(\theta_P) - u_\beta \cos(\theta_P)] \end{aligned} \tag{52}$$

REFERENCES

[1] Y. Shao and Y. Tang, "Fast evaluation of commutation failure risk in multi-infeed HVDC systems," *IEEE Trans. Power Syst.*, vol. 33, no. 1, pp. 646–653, Jan. 2018.
[2] E. Rahimi, A. M. Gole, J. B. Davies, I. T. Fernando, and K. L. Kent, "Commutation failure analysis in multi-infeed HVDC systems," *IEEE Trans. Power Del.*, vol. 26, no. 1, pp. 378–384, Jan. 2011.
[3] J. He, Y. Tang, J. Zhang, Q. Guo, J. Yi, and G. Bu, "Fast calculation of power oscillation peak value on AC tie-line after HVDC commutation failure," *IEEE Trans. Power Syst.*, vol. 30, no. 4, pp. 2194–2195, Jul. 2015.
[4] H. Xiao, J. Zhu, Y. Li, and X. Duan, "Efficient approach to quantify commutation failure immunity levels in multi-infeed HVDC systems," *IET Gener., Transmiss. Distrib.*, vol. 10, no. 4, pp. 1032–1038, Mar. 2016.
[5] D. Rimorov, I. Kamwa, and G. Joos, "Quasi-steady-state approach for analysis of frequency oscillations and damping controller design," *IEEE Trans. Power Syst.*, vol. 31, no. 4, pp. 3212–3220, Jul. 2016.
[6] T. Johnson and K. N. Shubhanga, "Response-type modelling of a two-terminal HVDC link for power system stability analysis," in *Proc. Innov. Power Adv. Comput. Technol. (i-PACT)*, Apr. 2017, pp. 1–6.
[7] P. Kundur, *Power System Stability and Control*. New York, NY, USA: McGraw-Hill Professional, 1994.
[8] G. Carpinelli, F. Gagliardi, M. Russo, and D. Villacci, "Generalised convertor models for iterative harmonic analysis in power systems," *IEE Proc.- Gener. Transmiss. Distrib.*, vol. 141, no. 5, pp. 445–451, 1994.
[9] S. D. Pekarek, O. Wasynczuk, E. A. Walters, J. V. Jatskevich, C. E. Lucas, N. Wu, and P. T. Lamm, "An efficient multirate simulation technique for power-electronic-based systems," *IEEE Trans. Power Syst.*, vol. 19, no. 1, pp. 399–409, Feb. 2004.
[10] P. Le-Huy, G. Sybille, P. Giroux, L. Loud, J. Huang, and I. Kamwa, "Real-time electromagnetic transient and transient stability co-simulation based on hybrid line modelling," *IET Gener., Transmiss. Distrib.*, vol. 11, no. 12, pp. 2983–2990, Aug. 2017.
[11] Y. Zhang, A. M. Gole, W. Wu, B. Zhang, and H. Sun, "Development and analysis of applicability of a hybrid transient simulation platform combining TSA and EMT elements," *IEEE Trans. Power Syst.*, vol. 28, no. 1, pp. 357–366, Feb. 2013.
[12] J. Mahseredjian, V. Dinavahi, and J. A. Martinez, "Simulation tools for electromagnetic transients in power systems: Overview and challenges," *IEEE Trans. Power Del.*, vol. 24, no. 3, pp. 1657–1669, Jul. 2009.
[13] J. R. Marti and J. Lin, "Suppression of numerical oscillations in the EMTP power systems," *IEEE Trans. Power Syst.*, vol. 4, no. 2, pp. 739–747, May 1989.
[14] T. Noda, K. Takenaka, and T. Inoue, "Numerical integration by the 2-stage diagonally implicit Runge-Kutta method for electromagnetic transient simulations," *IEEE Trans. Power Del.*, vol. 24, no. 1, pp. 390–399, Jan. 2009.
[15] M. Zou, J. Mahseredjian, G. Joos, B. Delourme, and L. Gérin-Lajoie, "Interpolation and reinitialization in time-domain simulation of power electronic circuits," *Electr. Power Syst. Res.*, vol. 76, no. 8, pp. 688–694, May 2006.
[16] B. K. Perkins, "Steady-state solution of the HVDC converter including AC/DC system interaction by a direct method," *IEEE Trans. Power Del.*, vol. 14, no. 4, pp. 1454–1460, Oct. 1999.
[17] M. O. Faruque, Y. Zhang, and V. Dinavahi, "Detailed modeling of CIGRÉ HVDC benchmark system using PSCAD/EMTDC and PSB/SIMULINK," *IEEE Trans. Power Del.*, vol. 21, no. 1, pp. 378–387, Jan. 2006.
[18] L. Yu, R. Li, and L. Xu, "Distributed PLL-based control of offshore wind turbines connected with diode-rectifier-based HVDC systems," *IEEE Trans. Power Del.*, vol. 33, no. 3, pp. 1328–1336, Jun. 2018.
[19] E. Hairer and G. Wanner, *Solving Ordinary Differential Equations II: Stiff and Differential-Algebraic Problems*, 2nd ed. Berlin, Germany: Springer, 1996.

CHONGTAO LI received the Ph.D. degree in electrical engineering from Xi'an Jiaotong University, Xi'an, China, in 2013. He is currently an Associate Professor of electrical engineering with Xi'an Jiaotong University. His research interest includes power system stability and control.

YONG ZHAO is currently a Senior Engineer with the Electric Power Research Institute, CSG, Guangzhou, China. His research interest includes power system stability.

FENG ZENG received the B.S. degree in electrical engineering from Xi'an Jiaotong University, Xi'an, China, in 2018, where he is currently pursuing the M.S. degree.

His research interest includes stability analysis and control of wind power systems.

ZHENGCHUN DU (Member, IEEE) was born in Shaanxi, China, in 1963. He received the B.S., M.S., and Ph.D. degrees in electrical engineering from Xi'an Jiaotong University, Xi'an, China, in 1983, 1986, and 1993, respectively. He is currently a Professor of electrical engineering with Xi'an Jiaotong University. His research interest includes power system stability and control.